



Shahid Chamran
University of Ahvaz

Journal of Applied and Computational Mechanics



Research Paper

Flow Regimes Characteristics of Water-crude Oil in a Rectangular Y-microchannel

Maxim I. Pryazhnikov^{1,2}, Andrey V. Minakov^{1,2}, Dmitriy V. Guzei^{1,2}, Andrey I. Pryazhnikov¹, Anton S. Yakimov¹

¹ Siberian Federal University, Krasnoyarsk, Russia, 79 Svobodny pr., Krasnoyarsk, 660041, Russian Federation, Email: MPryazhnikov@sfu-kras.ru

² Kutatadze Institute of Thermophysics, SB RAS, Address, Novosibirsk, 630090, Russian Federation, Email: AMinakov@sfu-kras.ru

Received October 05 2021; Revised November 25 2021; Accepted for publication December 10 2021.

Corresponding author: M. Pryazhnikov (MPryazhnikov@sfu-kras.ru)

© 2022 Published by Shahid Chamran University of Ahvaz

Abstract. The paper deals with the investigation of the flow regimes of water and crude oil in a Y-microchannel. Systematic experiments allow distinguishing four different types of water-oil flow regimes in studied microchannel, namely, plug regime, droplet regime, parallel regime, and the first-revealed chaotic regime, as well as defining the ranges of parameters corresponding to these regimes. The dependences of the water plug length and frequency of their formation in crude oil on various parameters are obtained, and universal correlations are derived. It was demonstrated that when determining the dimensionless plug lengths and the Strouhal number corresponding to droplet detachment, it is necessary to take into account not only the ratio of the dispersed and carrier phase flow rates but also the capillary number. The systematic numerical simulation of the considered flows is conducted using the VOF method. The conducted comparison of the computation and experimental results has shown that the numerical simulation qualitatively correctly predicts the characteristics of water and oil flows in the Y-type channel under consideration.

Keywords: Liquid-liquid flow, Y-junction, flow regimes, flow map, volume of fluid method (VOF).

1. Introduction

Interest in two-phase flows in microchannels has considerably increased over the last decade. This is not only due to the issues of fundamental science but also due to serious achievements in the field of practical applications. The two-phase flow regime in micro- and minichannels is widespread in industrial and technological devices that use gas-liquid flows or flows of immiscible liquids [1-5]. Besides, two-phase flows in microchannels are very widespread in various natural objects, such as oil-bearing fluid flows in porous media, flows in biological systems, and many others. In particular, studies of gas-liquid flows have become very widespread among the two-phase flows in microchannels. Interest in these applications leads to a lot of works carried out on this topic in past two decades [6-9].

Another important class of flows in microchannels is immiscible fluid flows. Such flows are very common in oil-bearing fluid flows in porous media, and are characterized by enhanced diversity of flow regimes. These regimes are caused by the predominance of interfacial interaction forces over the inertia and gravity forces due to the small characteristic size of the microchannel. The flows of immiscible liquids in microchannels have also been intensively studied over recent years [10-31]. At that, the data on flow regime maps for this class of flows in microchannels is significantly less than for gas-liquid flows. Currently, the following flow regimes of immiscible two-component flows in microchannels are revealed: droplet, plug, sliding-plug, stratified (parallel), serpentine, annular, and many intermediate regimes [12-22]. The flow regime depends on the balance of forces. In microchannels, these are usually interfacial tension, inertial, and viscous forces.

At the moment, there is no consensus on what parameters should be used to build map of flow regimes for two-phase flows in microchannels. In many, usually, earlier works, the flow velocities or flow rates of the phases were used to characterize the flow regimes [9-11]. It is also common to use the Reynolds number for classifying flow regimes [10]. In the investigation of Zhao et al. [15] the map of flow regimes is constructed relative to the Weber number (We), which is responsible for the balance of inertia and surface tension forces. In paper [16], the flow regimes of immiscible liquids were constructed as dependences on the capillary number Ca for the carrier phase, and the We number for the dispersed phase. In the work of Kashid et al. [17], to describe the liquid-liquid flow regimes in microchannels, it was proposed to use the Laplace number ($La = Re/Ca$) for the carrier phase and the dimensional criterion $Re \cdot d / \alpha$ for the dispersed phase, where d is the hydraulic diameter of the channel, α is the volume fraction of the dispersed phase. Often, the combination $Re^a We^b$ is used to describe the flow regimes, where a and b are different power exponents. An example of such a representation can be found in [18]. However, this kind of representation cannot



be considered universal. Apparently, the most general criterion for describing the immiscible liquids flow regimes in microchannels of rectangular cross-section today should be considered the criterion proposed by Yagodnitsyna et al. [19-20]. This is the product of the Weber and Ohnesorge numbers ($WeOh$). The Ohnesorge criterion establishes a relationship between viscous forces and surface tension forces. Thus, using the proposed criterion, it became possible to construct a relatively universal regime map for the flows of immiscible liquids in a T-microchannel. The results of numerical simulations performed by Minakov et al. [21] fully confirmed the existence of above-noted regimes. In work Darekar et al. [22], the flow regime maps for immiscible liquids in Y-type microchannel were constructed using different coordinates. It is noted that the use of We and $WeOh$ numbers is the most convenient when building such maps.

In addition to the properties of liquids, such as viscosity and interfacial tension, the flow regimes of two-phase flows in microchannels are most significantly influenced by the wetting conditions on the walls. By changing the contact angle on the channel wall, one can significantly change or shift certain flow regimes of two-phase flows in microchannels. However, there are still no models that could accurately predict the flow regime map, taking into account the wettability conditions of the wall surface. Creating such universal models is complicated by the fact that the behavior of the contact line on the microchannel walls in many cases cannot be described by the equilibrium value of the wetting angle [18, 23-25].

The immiscible liquid flows are of particular importance when solving problems of oil displacement during the flooding of reservoirs, whose pore space is represented by a network of microchannels of complex shape. Many methods of enhancing oil recovery are based on controlling the flow regimes of crude oil and displacement fluids. The improvement of oil recovery from a microporous medium depends on the flow structure in the pore space. The flow structure that occurs in a microporous medium depends on several parameters, namely, the geometry (the characteristic size and type of connections of the microchannels of the porous medium), the physical properties of the oil, and the displacement fluid used to improve oil recovery (density, viscosity, interfacial tension, and wetting angle). Currently, microfluidics is widely used to study flows during the crude oil displacement from a porous medium [26-31].

However, despite the relatively large number of works dealing with the investigation of crude oil flows in microporous media, systematic data on the flow regimes occurring there are still insufficient. The number of factors that affect the flow regimes in oil displacement is so large that requires studying them further. Besides, there are still many unsolved problems related to simulation methods of such flows, first of all, providing careful consideration of the interfacial tension forces, simulation of the contact line, and the surface wetting effects.

In this regard, the aim of the present work was a systematic experimental and numerical investigation of the water-crude oil flow in the Y-microchannel, and the determination of the main characteristics of these flows.

2. Experimental Materials and Methods

2.1 Properties of used liquids

The distilled water and light crude oil were used. Interfacial tension (IFT) and contact angle (CA) were measured with a tensiometer. A detailed description of the IFT and CA measurements is presented in our recent works [32-33]. Data variances in the experiments did not exceed 5%. The measurement of the viscosity was carried out using Brookfield viscometer [34], the measurement error was about 2%. The density was determined by measuring the mass with a precision balance and the volume using graduated beakers. The density determining error was about 1%. The density, dynamic viscosity, interfacial tension, and contact angle (water-oil-wall) of water and oil are shown in Table 1.

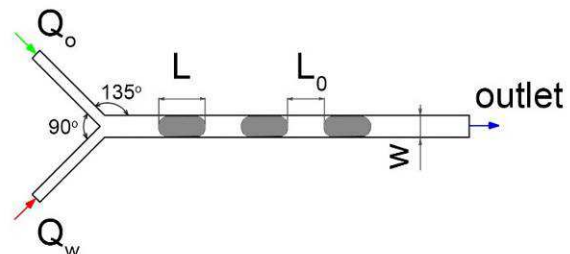
2.2 Chip and Y-type microchannel fabrication

The study was carried out using a chip with a Y-junction (Fig. 1). The microchannel outlet width w and height h were 500 and 200 microns, respectively, while the length was 20 mm. The microchannel inlet width were 325 microns each, while the length was 5 mm (schematic diagram in Fig. 1b).

The chip was made of PMMA (polymethylmethacrylate, Novattro, Russia) by milling [35] and thermal bonding [36]. Milling was performed using a ModelaMDX-40a miller (Roland, Japan) with a 0.2 mm diameter T2-02 double-pronged cutter (RDM, Russia) in a bath with distilled water. The cutting depth was 20 μm , step over – 50 μm , feed per tooth – 1 μm , cutting speed – 9.42 m/min. For thermal sintering, the PMMA plates of the chip were kept in a drying cabinet at a temperature of 140 °C for 10 min, and then pressed together under a pressure of 180 kPa, and cooled down for 5 min. Miniature threaded connections SMC M-3AU-2 (SMC, Japan) were used to connect polypropylene pipes with diameters ID of 1.2 and OD of 2 mm.



(a)



(b)

Fig. 1. Photo of a chip with a Y-type microchannel (a) and its schematic diagram (b).

Table 1. Properties of used liquids at 25°C.

Parameter	Water	Oil
Density, kg m ⁻³	997	826
Viscosity, mPa s	0.894	8.47
IFT, mN m ⁻¹		22.4
CA, deg		23.5

2.3 Experimental setup

The diagram of the experimental procedures is shown in Fig. 2. Oil and water are pumped into the PMMA chip with a Y-type microchannel using SP Lab02 syringe pumps (Baoding Shenchen Precision Pump Co., Ltd) (with a relative flow rate error of 0.5%). The microchannel was placed horizontally on the microscope slide table, equipped with a high-speed camera acA2000-165um-Baslerace (BaslerAG, Germany). The temperature controller (Meros TCU-100, Dolomite) was used in experiment. The microchannel inlets were connected to Hamilton syringes (Model number: 1005) by polypropylene tubes with ID of 1.2 mm and an OD of 2 mm. The volumetric flow rate of liquids Q was set at a certain value. A dispersion consisting of water and oil was formed in the Y-type microchannel. Flow pattern in microchannel was recorded by a high-speed camera, which saved the images to a computer for further analysis.

The liquid-liquid flow regime in the microchannel is affected by inertia, viscous, and surface tension forces. Dimensionless similarity criteria that characterize a particular flow regime are the Reynolds, Weber, and capillary numbers.

The Reynolds number is responsible for the ratio of the inertial forces to the viscous forces:

$$Re = \frac{\rho U D}{\mu} \quad (1)$$

where ρ is the density of the liquid; U is the characteristic velocity; D is the hydraulic diameter of the channel; μ is the dynamic viscosity of the liquid. Characteristic velocity is:

$$U = \frac{Q}{S} \quad (2)$$

where S is the cross-sectional area of the microchannel. The hydraulic diameter is defined as:

$$D = \frac{4S}{P} \quad (3)$$

where P is the perimeter of the microchannel cross-section. The hydraulic diameter of the microchannel was 286 microns.

The Weber number characterizes the balance between the inertia and surface tension forces:

$$We = \frac{\rho U^2 D}{\sigma} \quad (4)$$

σ is the surface tension.

The capillary number characterizes the ratio between the viscous and surface tension forces:

$$Ca = \frac{\mu U}{\sigma} \quad (5)$$

The ratio of the viscous forces to inertial and the surface tension forces is determined by the Ohnesorge number:

$$Oh = \frac{\mu}{\sqrt{\rho \sigma D}} \quad (6)$$

When constructing a flow regime map for liquids flowing in microchannels, the Reynolds number, the Weber number, and the product of Weber and Ohnesorge numbers are used most often:

$$WeOh = Ca\sqrt{We} = \sqrt{ReCa^3} \quad (7)$$

Experiments were conducted within a wide range of liquid flow rates and similarity numbers. The ranges of similarity criteria are presented in Table 2.

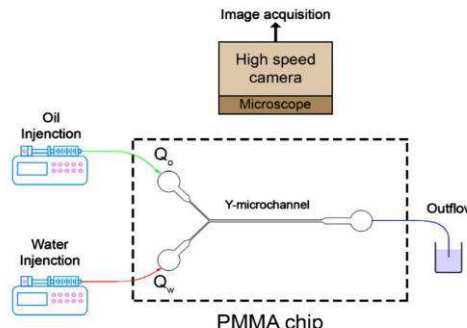


Fig. 2. Schematic diagram of the experimental setup.



Table 2. Ranges of experimental parameters.

Parameter	Water	Crude oil
Q [ml/h]	$2.5 \cdot 10^{-2} < Q_w < 6.6 \cdot 10^2$	$10^{-1} < Q_o < 55$
Re	$2.2 \cdot 10^{-2} < Re_w < 5.8 \cdot 10^2$	$7.7 \cdot 10^{-3} < Re_o < 4.2$
We	$6.1 \cdot 10^{-8} < We_w < 43$	$9.5 \cdot 10^{-8} < We_o < 2.8 \cdot 10^{-2}$
Oh	$1.2 \cdot 10^{-2}$	$1.17 \cdot 10^{-1}$
Ca	$2.8 \cdot 10^{-6} < Ca_w < 7.3 \cdot 10^{-2}$	$1.1 \cdot 10^{-4} < Ca_o < 5.7 \cdot 10^{-2}$

3. Mathematical Model

We consider a liquid-liquid flow in a microchannel. Only laminar flows were considered. The water and oil are immiscible. Each liquid (water and oil) is modeled as incompressible and Newtonian fluid. The VOF method, proposed by Hirt and Nichols [37], was used to simulate a water-oil flow in a microchannel. The marker function C keeps track of a volume fraction of the water C_w , the volume fraction of the oil C_o (in addition $C_w + C_o = 1$).

The properties (density and viscosity) can be determined based on a weighted average volume fraction of water:

$$\rho = \rho_w C_w + (1 - C_w) \rho_o \quad (8)$$

$$\mu = \mu_w C_w + (1 - C_w) \mu_o \quad (9)$$

here ρ , μ are the density and viscosity of fluid; subscript w – water, subscript o – crude oil (see Table 1).

The continuity equation describing the hydrodynamics of continuous media:

$$\frac{d\rho}{dt} + \nabla(\rho \vec{U}) = 0 \quad (10)$$

here \vec{U} is the mixture velocity vector, which is defined by solving a single-phase momentum equation:

$$\frac{d}{dt}(\rho \vec{U}) + \nabla(\rho \vec{U} \vec{U}) = -\nabla p + \nabla \cdot [\mu (\nabla \vec{U} + (\nabla \vec{U})^T)] + \vec{F}_{ca} \quad (11)$$

where p is the static pressure of the mixture, \vec{F}_{ca} is capillary forces.

The following transfer equation of marker function C is solved:

$$\frac{\partial C_w}{\partial t} + \nabla(C_w \vec{U}) = 0 \quad (12)$$

The capillary forces for immiscible liquid-liquid flow are very important. The continuum surface force (CSF), described by Brackbill et al. [38], algorithm was used to simulate surface tension. The vector of capillary forces is calculated as:

$$\vec{F}_{ca} = \sigma k \nabla C_w \quad (13)$$

where $k = -\nabla(\vec{n}/|\vec{n}|)$ is the surface curvature, where $\vec{n} = \nabla C_w$ is the normal vector to the interface between the phases.

The wall adhesion force was also taken into account by contact angle θ :

$$\vec{n} = \vec{n}_w \cos(\theta) + \vec{\tau}_w \sin(\theta) \quad (14)$$

here \vec{n}_w is normal to the wall vector, $\vec{\tau}_w$ is the tangential to the wall vector.

The measured physical properties (viscosity, density, interfacial tension, and contact angle) of crude oil-water systems were used in the calculations. These data are given in section 2.1.

The finite volume method was used to solve model equations (10-12). Pressure-velocity coupling was the semi-implicit method for pressure linked equations-consistent. The pressure staggering option was used to calculate continuity balance. Momentum discretization method was a second-order implicit scheme. A more detailed numerical technique that we use here can be found our papers [21, 39].

The 3D-computational domain corresponded to the geometry of the experimental Y-type microchannel. A structured grid consisting of 1,520,000 nodes was used in computations. For correct simulation of double-fluid plug flows in microchannels at least five compute nodes per film thickness are required [21]. The computation grid used in this paper met this criterion. The Courant number was set less than 2. The conducted methodological computations have shown that the used particularization of the computational grid and the choice of the time step allow obtaining solutions that are in good compliance with the experiment.

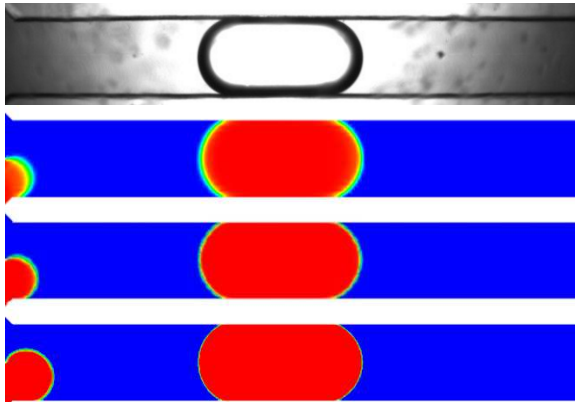
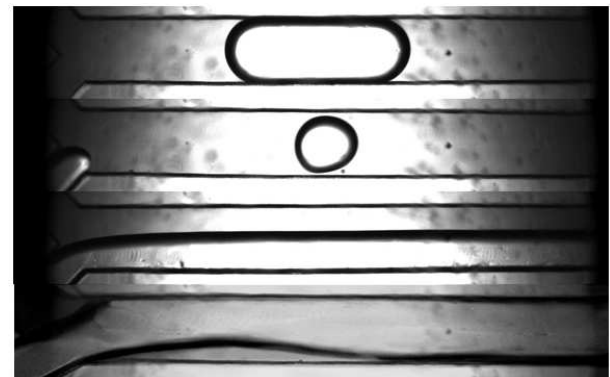
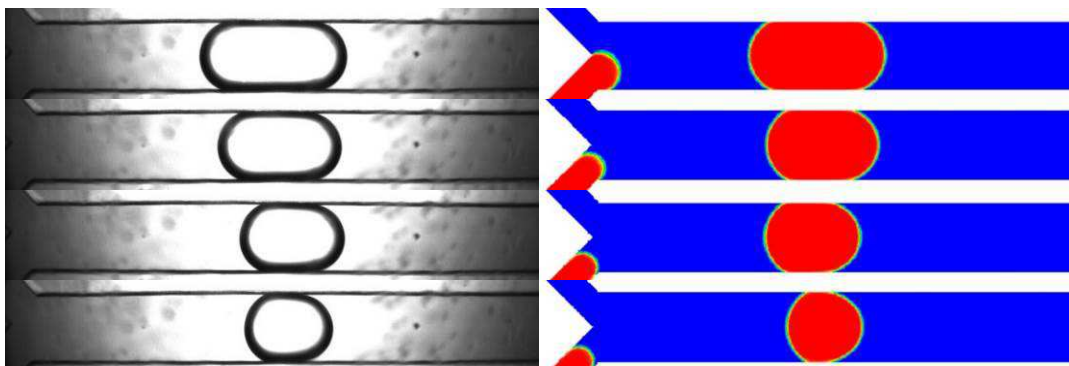
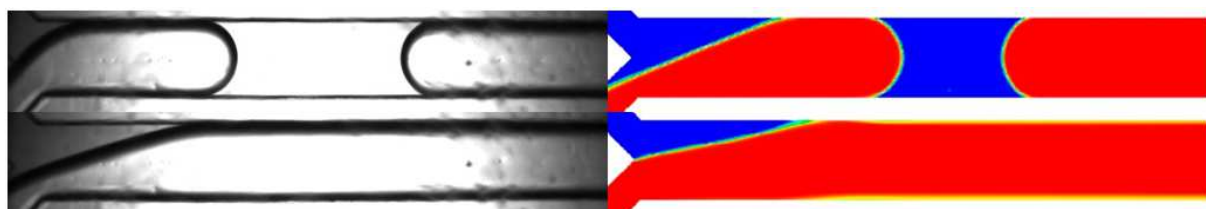
The boundary conditions at the mixer inlets included the mass flow rate corresponding to a steady velocity profile for given experimental conditions, while there were fixed pressure conditions for outflow. There were no-slip boundary conditions on the channel walls.

The effect of mesh detailing on the simulation result was carried out. The plug flow was considered as a test at an oil flow rate of 0.5 ml/h and water flow rate of 0.117 ml/h. Three computational grids with different details were used. The calculation results are shown in Figure 3 and in Table 3. Comparison of the simulation results for the length of the plug and the Plug detachment frequency showed that a computational grid containing 1,520,000 is sufficient to obtain a solution independent of further detailing. The computational mesh with medium detail was used for further numerical modeling.



Table 3. The mesh independence test.

Name	Nodes	Length of plug, mm	%	Plug detachment frequency, Hz	%
Low detail	190,000	0.69	19	0.39	6.3
Medium detail	1,520,000	0.82	3.5	0.408	2.5
High detail	5,130,000	0.84	1.2	0.412	1.7
Experiment	-	0.85	-	0.418	-

**Fig. 3.** Mesh independence test of plug flow regime at water flow rate of 0.117 ml/h, and oil flow rate of 0.5 ml/h.**Fig. 4.** Various flow regimes. From top to bottom: plug regime, droplet regime, parallel regime, chaotic regime.**Fig. 5.** Plug regime at $Q_w = 0.117$ ml/h. Oil flow rate (from top to bottom): 0.5, 3.1, 5.5, and 10 ml/h.**Fig. 6.** The regime of elongated plugs at $Q_w = 1.168$ and 11.68 ml/h for top and bottom figures respectively, $Q_o = 0.5$ ml/h.

4. Results and Discussions

As a result of a systematic experimental study, four different types of water-oil flow regimes in the Y-type microchannel were revealed, namely, plug, droplet, parallel and chaotic. Typical images of these regimes are shown in Fig. 4. A description of each flow regime is given below.

4.1 Plug flow

The plug flow regime is realized at low water and oil velocities. In all experiments, water plugs are formed in this regime. Oil is a continuous phase since oil wets the channel walls better. Water acts as a dispersed phase. The water plug occupies almost the entire cross-section with a very thin film of oil between the water plug and the microchannel wall (Fig. 5-7). At a constant water velocity, a decrease in the length of the plug was observed with an increase in oil velocity. The same trend was observed at a constant oil velocity, but at a decrease in water velocity. The plug regime of the water-oil flow in the Y-type microchannel is implemented within the following ranges of similarity criteria: $Re_w < 10$ and $Re_o < 1.3$, $We_w < 1.3 \cdot 10^{-2}$ and $We_o < 2.4 \cdot 10^{-2}$, $Ca_w < 1.3 \cdot 10^{-2}$ and $Ca_o < 1.8 \cdot 10^{-2}$.



Figures 5-6 show photos of the plugs formed in experiments and numerical simulation of the water-oil flow by the VOF method. The VOF method describes the shape of the plugs qualitatively well. Conducted tests have shown that the numerical computation well describes the experimental data on the plug shape, length, and velocity, as well as the film thickness, and the distance between the plugs within a wide range of dispersing and carrier phase flow rates.

At very low oil flow rates, formed plugs are elongated (Fig. 6). The characteristic length of elongated plugs is much greater than the distance between them. Figure 6 shows the elongated plug flow regime at a fixed oil flow rate of 0.5 ml/h and two values of water flow rates of 1.168 and 11.68 ml/h, respectively. As is obvious, the computation results well reproduce the plug shape and size in these regimes as well.

From a practical viewpoint, an important characteristic of such a flow is information about the length and distances between the plugs. In most works, attention is focused on studying effect of various parameters on the length of plugs in microchannels of various shapes [40-45]. However, universal correlations to predict the length of the plugs have not yet been created. Figure 7 shows the relative length of the plugs and the relative distance between the plugs (both quantities are reduced to the hydraulic diameter of microchannel) depending on the ratio of water and oil flow rates. The results of numerical simulation for the corresponding experimental regimes are presented in the same Fig. 7. As already mentioned, the results of the computations are in good quantitative compliance with the experimental data on the relative length of the plugs and the distance between them. However, as can be seen, the obtained data are poorly generalized by the dependence containing only the ratio of the dispersed and carrier liquid flow rates.

The data obtained were compared with calculations by the known empirical correlations. One of the first correlations describing plug length was the correlation proposed by Garstecki et al. [40] for a gas-liquid flow in a T-type microchannel:

$$\frac{L}{D} = 1 + \alpha \frac{Q_d}{Q_c} \quad (14)$$

where α is the constant, whose value depends on the geometry of the T-junction. In various works, α varies within the range from 1 to 1.5.

A comparison with our data shows that at $\alpha=1$ equation (14) does not describe the experimental data well (Fig. 7a). In addition to equation (14), the correlation proposed by Xu et al.[41], which additionally takes into account the capillary number of the carrier phase, was also considered in the same work:

$$\frac{L}{D} = \varepsilon + k \left(\frac{Q_d}{Q_c} \right)^\alpha \left(\frac{1}{Ca_c} \right)^\beta \quad (15)$$

where ε , k , α , β are the parameters of equation (11). In consequence of the experimental data analysis, the following parameters of Eq. (15) were obtained for the plug flow regime: $\varepsilon = 1.72$, $k = 1.45$, $\alpha = 0.525$, $\beta = 0.138$.

Comparison of the plug length, calculated by Eq. (14) and Eq. (15) is shown in Fig. 8a. The conducted analysis has shown that taking into account the capillary number allows predicting the length of the plug much more accurately. Figure 8b shows the dependence of the plug length reduced to the capillary number L^* , taking into account the parameters of Eq. (15), which depends only on the ratio of water and oil flow rates:

$$L^* \left(\frac{Q_w}{Q_o} \right) = \left(\frac{\frac{L}{D} - \varepsilon}{k \cdot Ca_o^{-\beta}} \right)^{1/\alpha} \quad (16)$$

As can be seen, this correlation generalizes the obtained experimental data very well.

In addition to Eq. (14) and Eq. (15), several other empirical correlations describing the plug length in the concerned flow regime are available as well (Table 4). These correlations were obtained for microchannels of various types and shapes. In most cases, a T-type microchannel was considered. At present, data on the Y-type microchannel is very little.

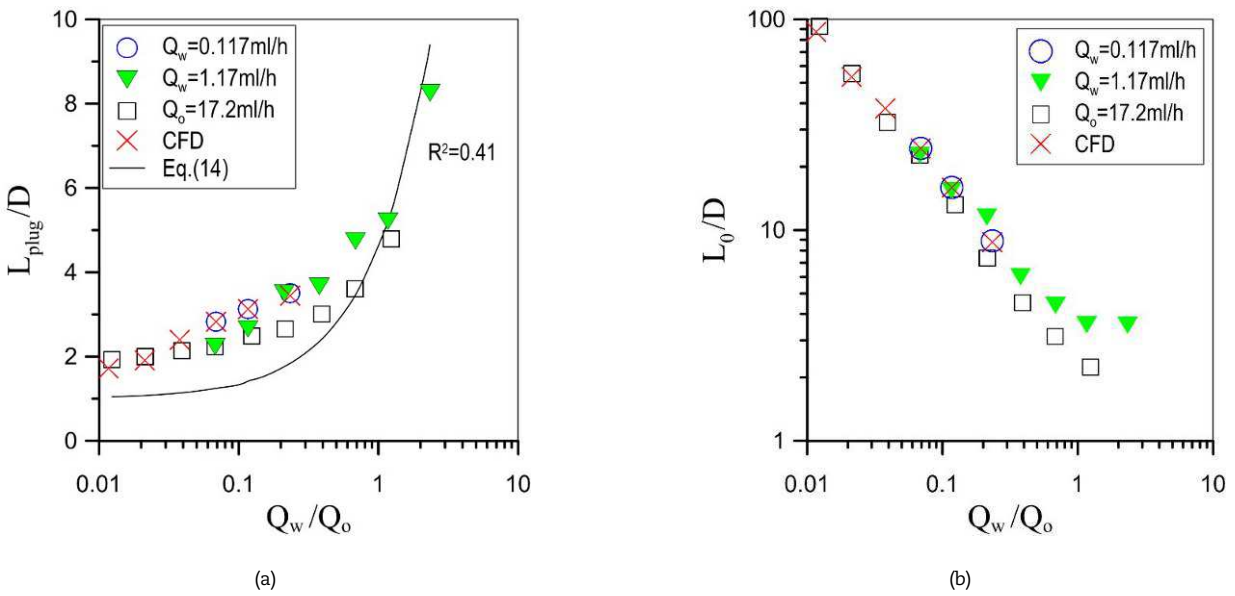


Fig. 7. Dependence of the relative plug length (left) and the relative distance between the plugs (right) on the ratio of water and oil flow rates.



Table 4. Correlations of the plug length.

Correlation	Flow	Junction type	Channel	Range	Reference
$\frac{L}{D} = 1 + \alpha \left(\frac{Q_d}{Q_c} \right)$	Liquid-gas	T	Rectangular	$Ca < 10^{-2}$	Garstecki et al. [40]
$\frac{L}{D} = 1 + 1.45 \left(\frac{Q_d}{Q_c} \right)$	Liquid-liquid	T	Rectangular	$4.8 \cdot 10^{-4} < Ca < 1.16$	Minakov et al. [21]
$\frac{L}{D} - \varepsilon = k \left(\frac{Q_d}{Q_c} \right)^\alpha Ca^\beta$	Liquid-liquid	T	Rectangular	$10^{-4} < Ca < 0.3$	Xu et al. [41]
$\frac{L}{D} = 0.757 \left(\frac{Q_d}{Q_c} \right)^{0.512} Ca^{-0.273}$	Liquid-liquid	T	Circular	$0.0224 < Ca < 0.299$	Li and Angeli [42]
$\frac{L}{D} = 2.19 \left(\frac{Q_d}{Q_c} \right)^{0.91} Re_d^{-0.72} We_d^{0.064}$	Liquid-liquid	Cross	Square	$Ca < 0.133$	Cao et al. [43]
$\frac{L}{D} = 1.3 \varepsilon^{0.07} (1 - \varepsilon)^{-1.01} We^{-0.1}$	Gas-liquid	Y	Square, circular, rectangular	$0.06 < \varepsilon < 0.85$ $0.1 < We < 26$	Sobieszuk et al. [44]
$\frac{L}{D} = 0.72 \left(\frac{Q_d}{Q_c} \right)^{0.14} Ca^{-0.15} \left(\frac{L}{D} < 2.35 \right)$	Liquid-liquid	T	Circular	$10^{-3} < Ca < 10^{-2}$	Fu et al. [45]
$\frac{L}{D} = 0.30 \left(\frac{Q_d}{Q_c} \right)^{0.23} Ca^{-0.042} \left(\frac{L}{D} < 2.35 \right)$					

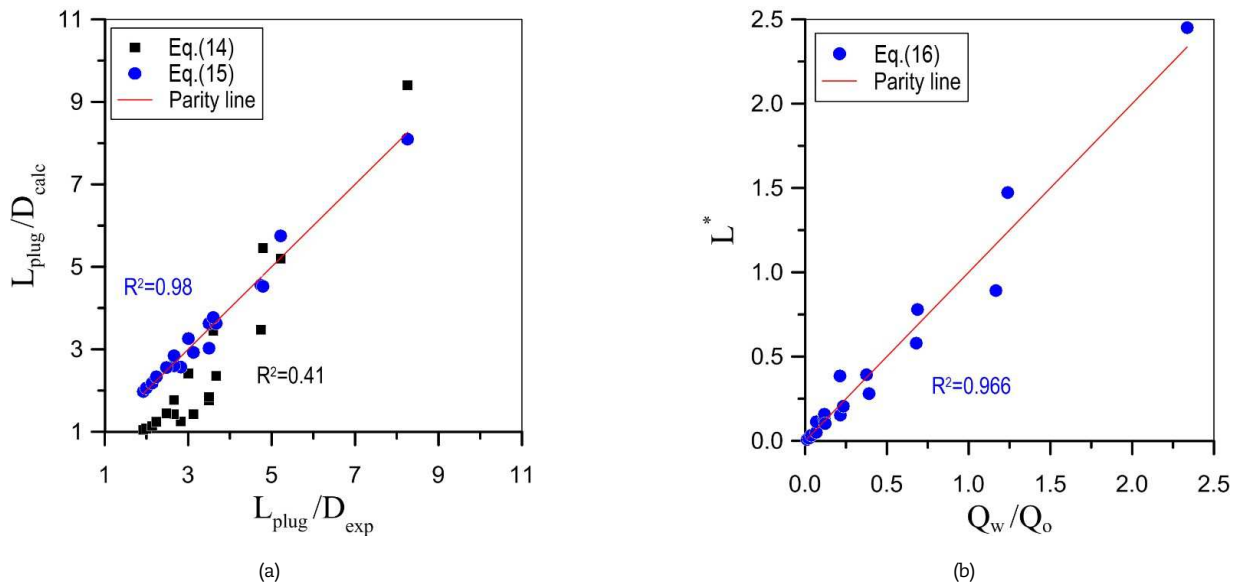
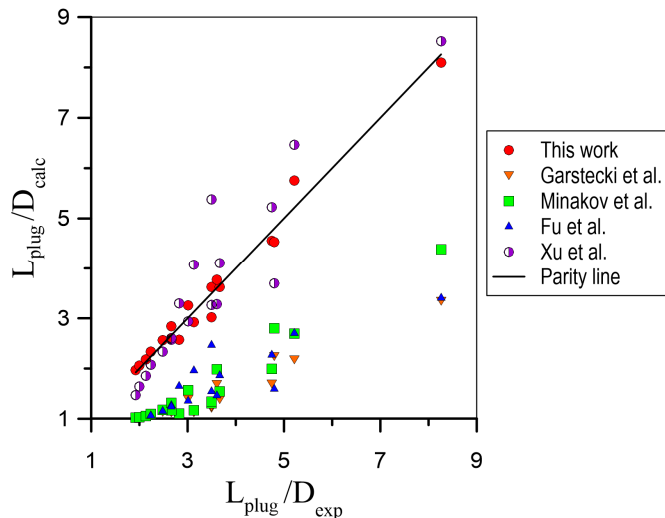
Fig. 8. (a) Dependence between the experimental and calculated relative plug length; (b) The dependence of L^* on the ratio of water and oil flow rates.

Fig. 9. Comparison of the dimensionless plug length obtained experimentally with calculations by the correlations listed in Table 4.



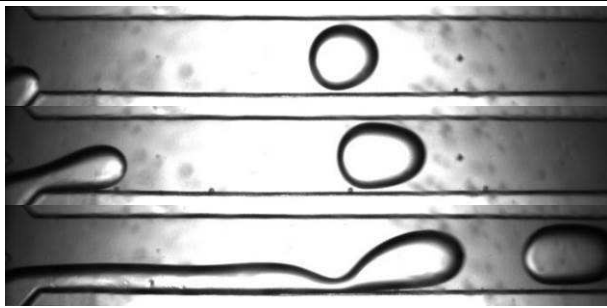


Fig. 10. Droplet regime at $Q_o = 54.5 \text{ ml/h}$. Water flow rate (from top to bottom): 1.168, 11.68, 36.93 ml/h .

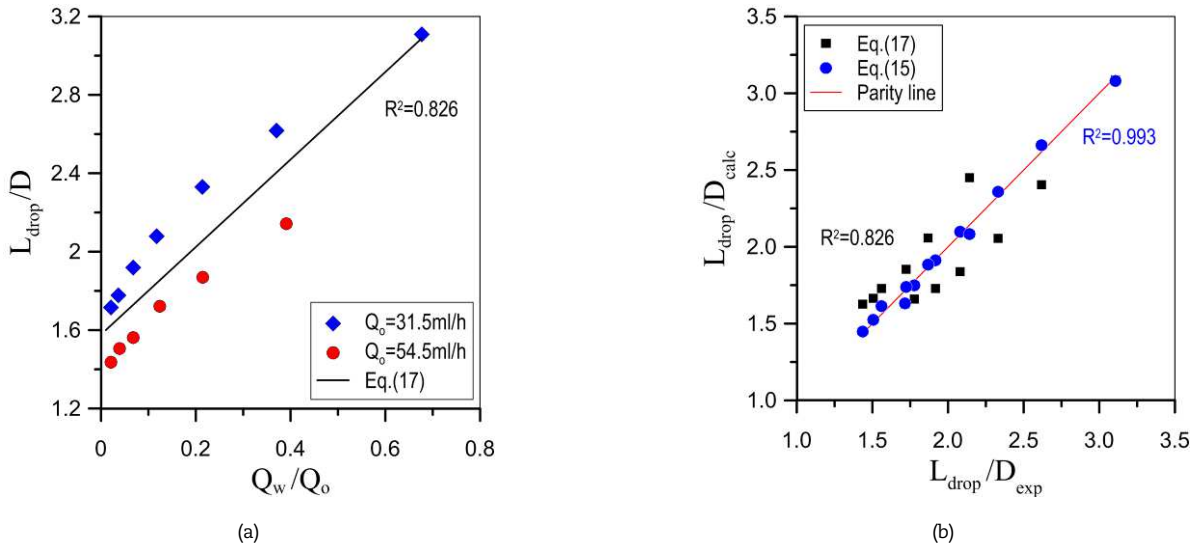


Fig. 11. (a) The relative size of the droplets vs the ratio of water and oil flow rates. (b) Comparison of the dimensionless droplet length obtained experimentally with correlations.

Figure 9 shows the comparison of the obtained experimental data on the dimensionless plug length with the known correlations of various researchers. The best match of experiments is obtained using the correlation proposed by Xu et al. [41].

4.2 Droplet flow

Typical photos are presented in Figs. 10. In this regime, the size of the water droplets is smaller than the size of the microchannel. This regime is implemented at high flow rates of the carrier medium (oil) and low flow rates of the dispersed phase (water): $Re_w < 10$ and $Re_o > 1.3$, $We_w < 1.3 \cdot 10^{-2}$ and $We_o > 2.4 \cdot 10^{-2}$, $Ca_w < 1.3 \cdot 10^{-2}$ and $Ca_o > 1.8 \cdot 10^{-2}$. The fragmentation of water into droplets is associated with a strong influence of inertia forces that occur at high water flow rates. The droplet flow regime is widely used in the problems of oil displacement from a porous medium.

It should be noted that currently there are practically no empirical correlations that would determine the dependence of the droplet size on various flow parameters in the microchannel. The minimum size of the droplets is usually less than the microchannel width, in contrast to plugs, whose length is comparable to the width of the microchannel or is much larger. By analogy with the plug flow regime, we present the dependence of the dimensionless length of the droplets on the ratio of water and oil flow rates in the following form:

$$\frac{L}{D} = A + B \frac{Q_w}{Q_o} \quad (17)$$

where A and B are the fitting parameters of the equation. At that, in contrast to the plug regime, the coefficient A is less than 1.

However, it was revealed that for the droplet regime, like for the plug regime, the dimensionless length of the droplets cannot be well described by a linear dependence on the ratio of the flow rates of the dispersed and carrier phases (Fig. 11a). As one can see in Fig. 11a, the length of the droplets depends not only on the ratio of the dispersed and carrier phase flow rates but also on the oil flow rate. Therefore, applying correlations like equation (17) gives a poor result. In turn, taking into account the capillary number using Eq. (15) allows well describing experimental data not only for the plug regime but also for the droplet regime (Fig. 11b). As a result, the following parameters of Eq. (15) were set for the droplet flow regime: $\varepsilon = 1.17$, $k = 0.0926$, $\alpha = 0.412$, $\beta = 0.936$. As can be seen, equation (15) with these parameters describes the experimental data very well.

Another important characteristic of the droplet flow regime is the droplet detachment frequency f . The dimensionless criterion that characterizes droplet detachment is the Strouhal number $St = f \cdot D / U_{mix}$ (here U_{mix} is the total velocity of water and oil). The droplet detachment frequency and the Strouhal number are presented in Fig. 12 depending on the flow rate ratios. In the beginning, we will use the standard representation of the Strouhal number depending on the ratio of flow rates expressed in power form (Fig. 12b):

$$St = K \left(\frac{Q_w}{Q_o} \right)^n \quad (18)$$

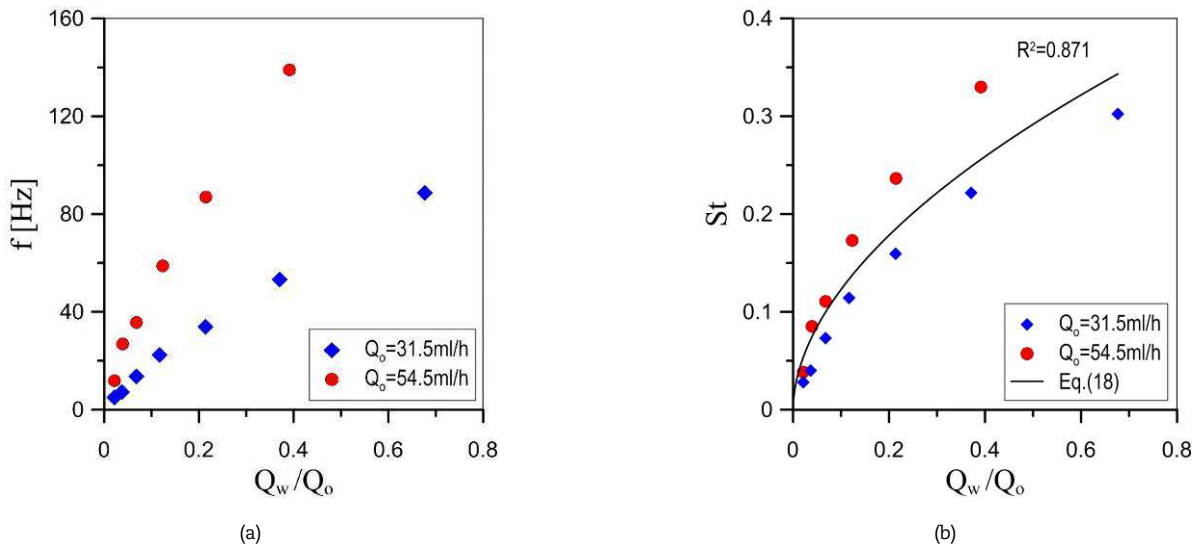


Fig. 12. Dependence of the droplet detachment frequency (left) and the Strouhal number (right) on the ratio of water and oil flow rates.

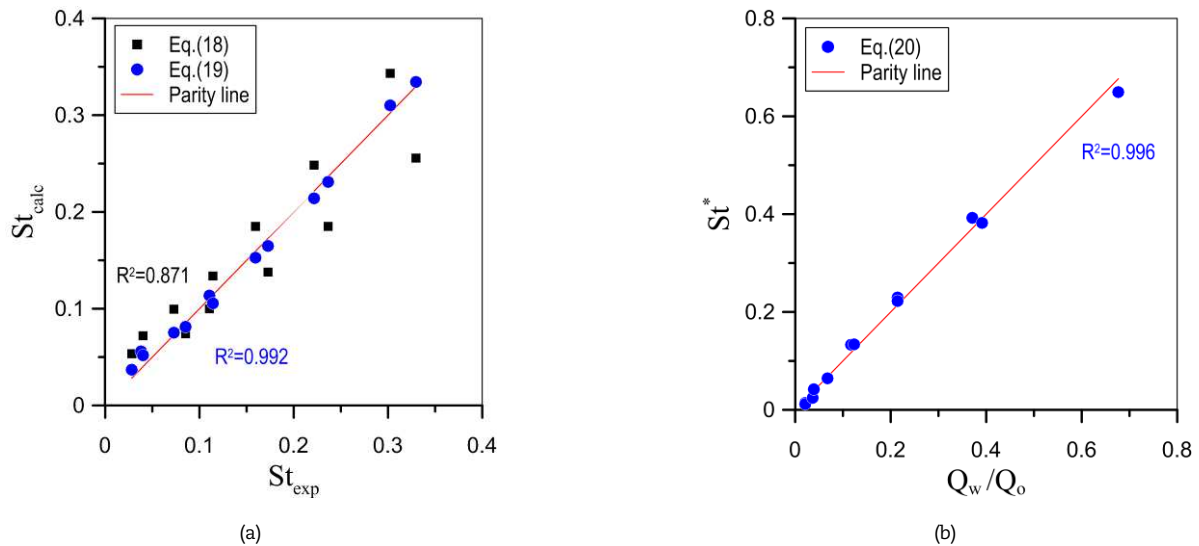


Fig. 13. (a) Comparison of the calculated and experimental Strouhal number; (b) The dependence of the Strouhal number on the ratio of water and oil flow rates.

where $K = 0.423$ and $n = 0.538$ are the adjusting coefficients of equation (18). As can be seen, the Strouhal number is also poorly described by the dependence on the ratio of the dispersed and carrier phase flow rates. The coefficients K and n in equation (18) differ for different oil flow rates. Accordingly, the correlation (18) cannot be considered universal.

Let take into account the capillary number of the carrier phase, as it was done for the dimensionless length of the plug:

$$St = K \left(\frac{Q_w}{Q_o} \right)^{n_1} \left(\frac{1}{Ca_o} \right)^{n_2} \quad (19)$$

where $k = 5.11$, $n_1 = 0.615$, $n_2 = 0.753$ are the adjusting coefficients of equation (19).

Next, we transform the Strouhal number expressed by Eq. (19) into the linear dependence on the dimensionless flow rate:

$$St^* \left(\frac{Q_w}{Q_o} \right) = \left(\frac{St}{k(1/Ca)^{n_2}} \right)^{1/n_1} \quad (20)$$

There is very good compliance of experimental data and correlation (20) (see Fig. 13). Thus, it was demonstrated that when determining the Strouhal number characterizing droplet detachment, it is necessary to take into account not only the ratio of the water and oil flow rates but also the capillary number.

Next, the average velocity of water droplets in the oil was measured. Figure 14 shows experimental data for the average droplet velocity as a function of the mixture velocity U_{mix} . As one can see, the velocity of the droplets is proportional to the mixture velocity. The analysis has shown that the best correlation between the droplet velocity and the mixture velocity has the power form $U_{\text{drop}} = 1.425 \cdot U_{\text{mix}}^{1.242}$.



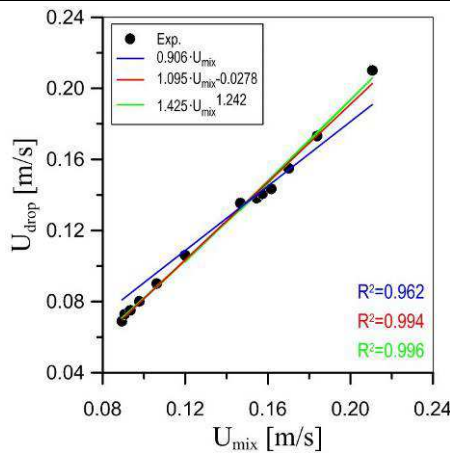


Fig. 14. Dependence of the average droplet velocity on the mixture velocity.

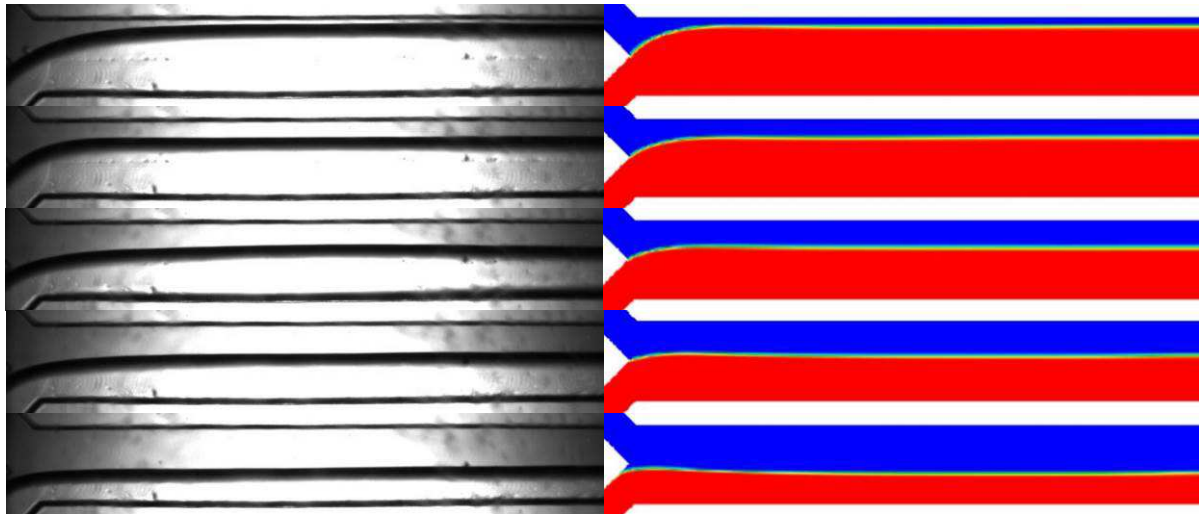
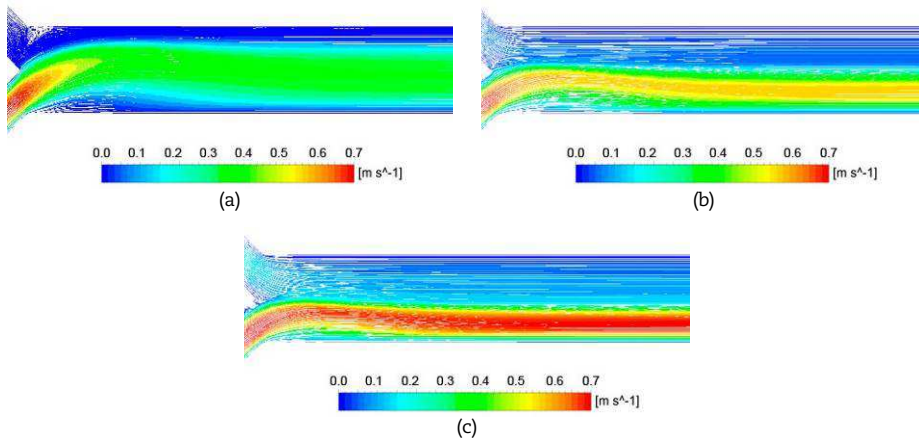
Fig. 15. Parallel regime at $Q_w = 36.9 \text{ ml/h}$. Oil flow rate (from top to bottom): 0.5, 1.0, 1.7, 3.1, 5.5, 10, 17.2 ml/h.

Fig. 16. Velocity vector field for different oil flow rates (water flow rate of 36.9 ml/h): a) 0.5; b) 5.5; c) 17.2 ml/h.

4.3 Parallel flow

At higher flow rates of water and oil, a parallel regime is observed. Both phases flow past each other without forming plugs or droplets, and not being mixed. Typical photos of the parallel regime are shown in Fig. 15. This regime is implemented at the following parameters: $Re_w > 10$, $We_w > 1.3 \cdot 10^{-2}$, $Ca_w > 1.3 \cdot 10^{-2}$. The calculation results were compared with the experimental data in the parallel flow regime at a water flow rate of 36.9 ml/h. The oil flow rate ranged from 0.5 to 17.2 ml/h. A comparison of the experimental photos with the calculation results is shown in Fig. 15. As the oil flow rate increases, the water/oil contact interface shifts along the channel cross-section. The position and shape of the contact interface are well described using a calculation technique based on the VOF method.

Figure 16 shows the calculated velocity fields in the microchannel for the water/oil flow in a parallel regime at different oil flow rates. The analysis of the obtained velocity fields shows that because the thickness of the layers in the mixing channel is different, the liquids move at essentially different velocities.

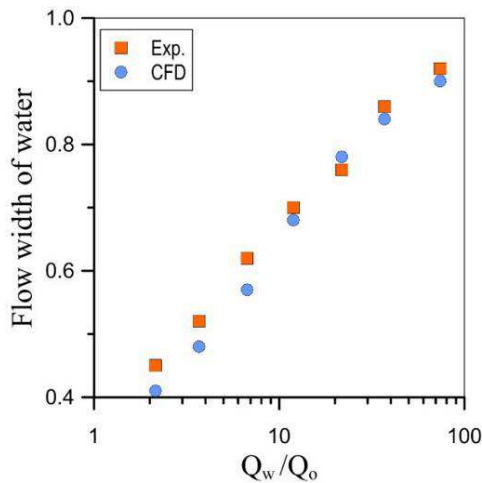


Fig. 17. The ratio of the water and oil layer thicknesses depending on the oil flow rate.

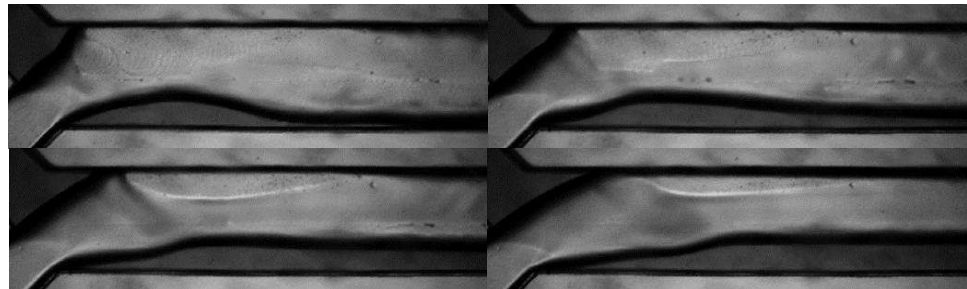


Fig. 18. Chaotic flow at a $Q_w = 660$ ml/h. Oil flow rate (from right to left, from top to bottom): 10, 17.2, 31.5, 54.5 ml/h.

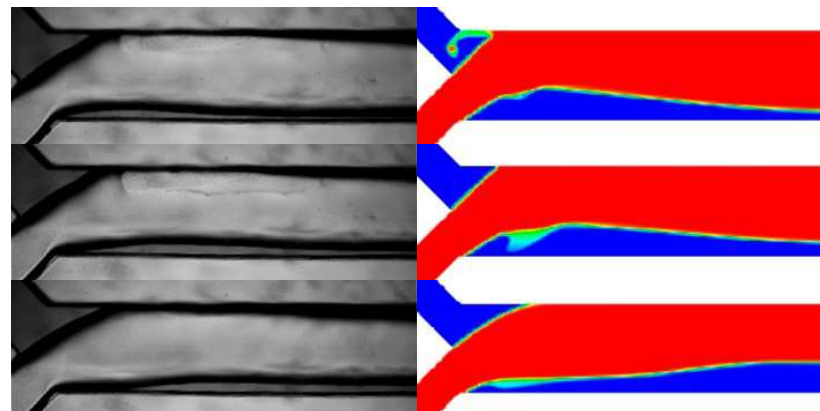


Fig. 19. Chaotic flow at $Q_w = 369.3$ ml/h. Oil flow rate (from right to left, from top to bottom): 3.1, 5.5, 10, 31.5 ml/h.

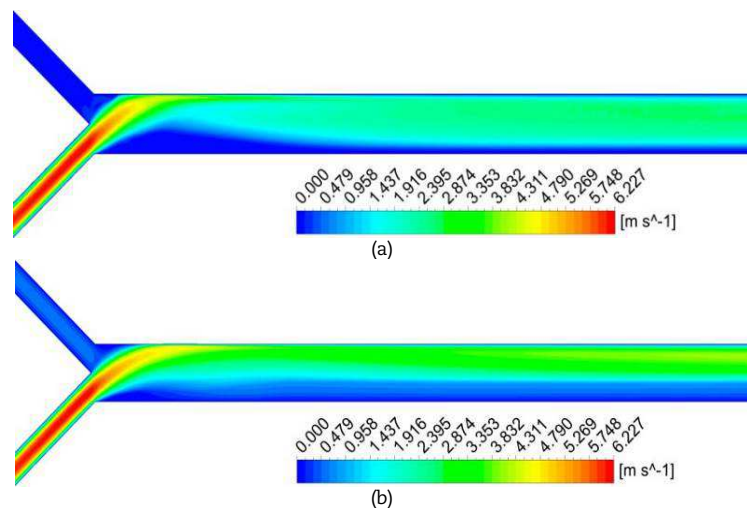


Fig. 20. Velocity field isolines in the microchannel at different oil flow rates: a) 3.1 ml/h; b) 31.5 ml/h.



Figure 17 shows a comparison of the experimental data with the calculation results for the ratio of the water and oil layer thicknesses depending on the oil flow rate (water flow rate of 36.9 ml/h). As is seen, good compliance has been achieved between experimental and calculation data.

4.4 Chaotic flow

With a further increase in water flow rate, the parallel flow regime changes to chaotic flow (Figs. 18-19). This regime is implemented at very high water and oil flow rates: for water $Re_w > 3.3 \cdot 10^2$, $We_w > 13$ and, $Ca_w > 4.1 \cdot 10^{-2}$, for oil – $Re_o > 2.4 \cdot 10^{-1}$, $We_o > 7.8 \cdot 10^{-4}$, $Ca_o > 3.3 \cdot 10^{-3}$. The chaotic flow regime was studied in detail at a constant water flow rate of 369.3 ml/h, while the oil flow rate varied within the range from 3.1 to 31.5 ml/h. Although such regimes are not typical for flows in microporous media, from a fundamental standpoint, this regime is of certain interest. In this flow regime, the water and oil flow overturn in the mixing channel and then flow in the stratified regime along the opposite walls. The best way to understand the flow structure in this regime is to use numerical simulation results. But first, let's compare the simulation results with the experiment. Such a comparison is shown in Fig. 19. As can be seen, in general, there is quite good qualitative compliance. Figures 20-21 show the calculated isolines of the velocity field and the flow structure in different sections of the microchannel for oil flow rates of 3.1 and 31.5 ml/h. At the junction, where the water and oil flows enter the main channel, water and oil flows intersect with each other, and the flow overturns. Similar behavior was observed in the single-phase flow of liquids in the T-type microchannel. The results of systematic studies of single-phase flow in this microchannel at high Reynolds numbers can be found in [46-47]. Due to the development of the secondary Dean flow, a pair of symmetric horseshoe vortices are formed, that decay in the microchannel. Moreover, each of these vortices is inside the same fluid (water or oil). Starting from the Reynolds number of approximately 145, a pair of horseshoe-shaped vortices unfolds at an angle of 30° to the central longitudinal plane of the microchannel, which leads to attenuation of one of the vortices and intensification of the other. A similar situation is generally observed in the case of a two-component flow in the Y-channel (Fig. 18-21). Liquids in the mixing channel are also overturned. And further, the flow continues running in a stratified regime.

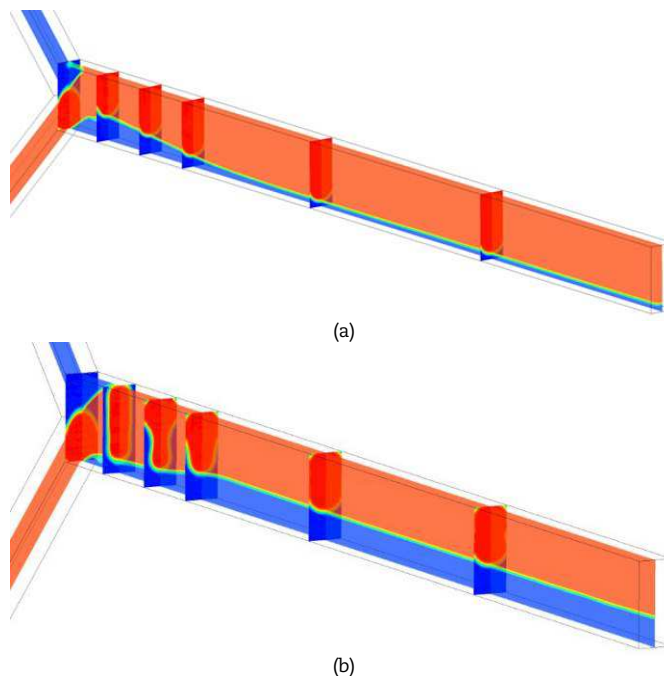


Fig. 21. Phase distribution in the microchannel at an oil flow rate equal to 3.1 (a) and 31.5 ml/h (b).

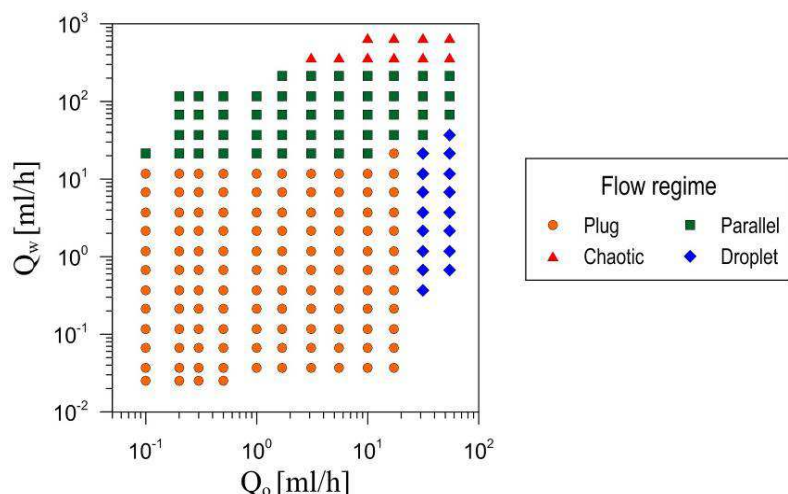


Fig. 22. Water-oil flow regime map in the coordinates of water and oil flow rates (left) and Reynolds numbers (right): green squares – parallel regime, orange circles – plug regime, blue rhombs – droplet regime, red triangles – chaotic regime.

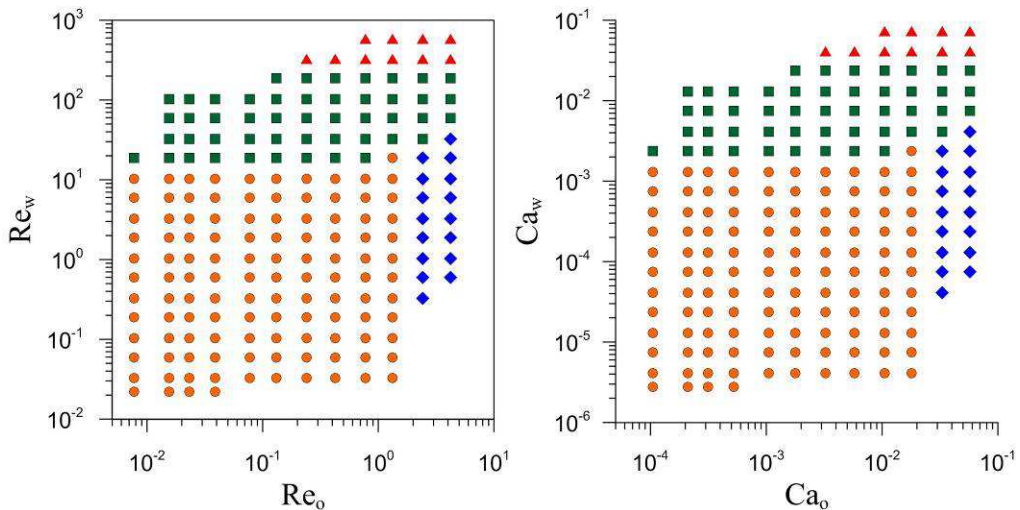


Fig. 23. Water-oil flow regime map in the coordinates of the Reynolds numbers (left) and capillary numbers (right); green squares – parallel regime, orange circles – plug regime, blue rhombs – droplet regime, red triangles – chaotic regime.

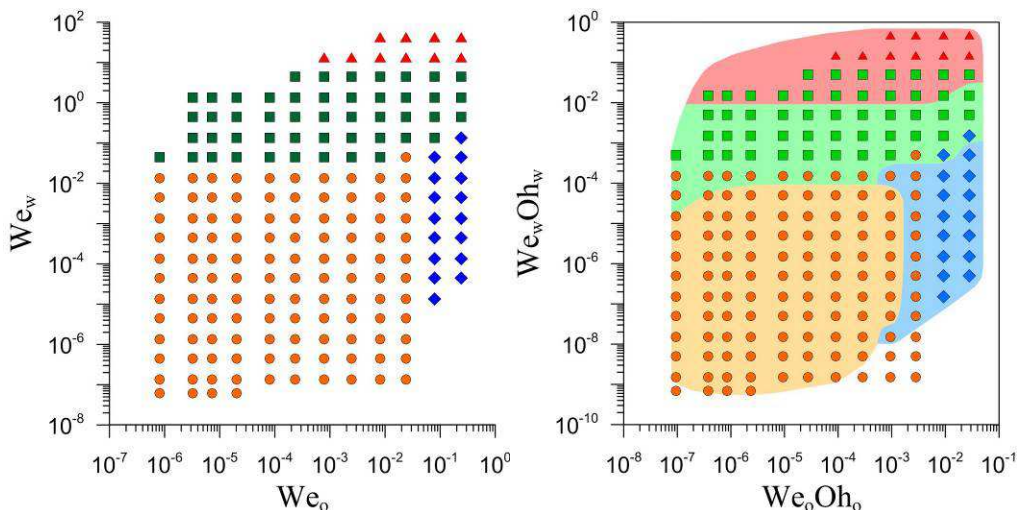


Fig. 24. Water-oil flow regime map in the coordinates of the Weber number (left) and the $We_{o,0}Oh_w$ product (right). Symbols correspond to experiments: green squares – parallel regime, orange circles – plug regime, blue rhombs – droplet regime, red triangles – chaotic regime; color shading – numerical simulation.

4.5 Flow regime map

To describe the ranges of the existence of different flow regimes, it is very important to build flow regime maps. As already mentioned in the introduction, currently, there is no consensus on what parameters should be used to build flow regime maps for two-phase flows in microchannels. In many, usually, earlier works, the velocities or flow rates of the phases were used to characterize the flow regimes. It is also common to use the Reynolds, Weber, and capillary numbers for the carrier and dispersed phases to classify flow regimes [9-16]. Combinations of numbers in various degrees $Re^a We^b$ are also used often to describe flow regimes [18]. Apparently, the product of the Weber and Ohnesorge numbers $We_{o,0}Oh_w$ is considered today the most common criterion to describe the immiscible liquids flow regimes in rectangular microchannels [19-20, 22].

Figures 22-24 show the obtained flow regime map in the Y-type microchannel in the most common coordinates.

Figure 24b shows a flow regime map in the coordinates of $We_{o,0}Oh_w$ numbers based on experimental data and numerical simulation results (symbols are experimentally observed regimes, shadings correspond to calculated regimes). As is obvious, the numerical simulation reproduces all the flow regimes obtained in the experiment within the entire considered range of oil and water flow rates. However, the flow regime boundaries corresponding to the numerical simulation are somewhat shifted. The calculation slightly delays the onset of the next regime compared to the experiment. Nevertheless, the calculated and experimental flow regime maps are very close. This allows using numerical simulations to build flow regime maps in microchannels.

5. Conclusions

- The paper presents an experimental and numerical study of the water-oil flow regimes in a rectangular Y-type microchannel.
- As a result of a systematic study, four different types of water-oil flow regimes in the Y-type microchannel were revealed, namely, plug, droplet, parallel, and chaotic.
 - The parametric ranges of the existence of these flow regimes are determined, and observed flow regime maps are constructed in different coordinates.
 - The effect of the droplet and plug flow regime parameters on the length, velocity, and frequency of water plug formation in crude oil are revealed.



- It was demonstrated that when determining the dimensionless plug lengths and the Strouhal number corresponding to droplet detachment, it is necessary to take into account not only the ratio of the dispersed and carrier phase flow rates but also the capillary number.
- Universal correlations defining these dependencies were derived.

For the plug flow regime ($Ca_w < 1.3 \cdot 10^{-3}$ and $Ca_o < 1.8 \cdot 10^{-2}$):

$$\frac{L}{D} = \varepsilon + k \left(\frac{Q_d}{Q_c} \right)^\alpha \left(\frac{1}{Ca_c} \right)^\beta,$$

where $\varepsilon = 1.72$, $k = 1.45$, $\alpha = 0.525$, $\beta = 0.138$.

For droplet flow regime ($Ca_w < 4.1 \cdot 10^{-3}$ and $Ca_o > 3.3 \cdot 10^{-2}$):

$$\frac{L}{D} = \varepsilon + k \left(\frac{Q_d}{Q_c} \right)^\alpha \left(\frac{1}{Ca_c} \right)^\beta,$$

where $\varepsilon = 1.17$, $k = 0.0926$, $\alpha = 0.412$, $\beta = 0.936$.

The Strouhal number corresponding to droplet formation:

$$St = k \left(\frac{Q_w}{Q_o} \right)^{n_1} \left(\frac{1}{Ca} \right)^{n_2},$$

where $k = 5.11$, $n_1 = 0.615$, $n_2 = 0.753$.

A detailed numerical simulation of the water-oil flow in the Y-type microchannel has been performed. Many works are devoted to the study of water-oil flow in the microchannel and flow regime map. However, in contrast to our work, in most cases the researchers considered very small values of capillary numbers and the results were obtained on model fluids. In our work, the flow regimes of crude oil have been investigated. In addition, we have significantly advanced in terms of the capillary number up to $Ca < 0.1$. Of course, such high values of the capillary number are not typical for terrigenous sandstone reservoirs. However, the results obtained will be of great interest for fractured carbonate rocks. In such rocks, the considered flow regimes are realizable, but currently there are practically no data on these regimes. In our work, such systematic data were obtained for the first time. The flow structure in the considered regimes was studied using numerical simulation. The results of numerical simulations confirmed the existence of the flow regimes detected experimentally. The comparison of the calculation and the experiment has shown that the calculation in all cases qualitatively correctly predicts the characteristics of water and oil flows in the considered Y-type microchannel. Conducted computations have shown that the numerical simulation describes well the experimental data in terms of the shape, length, and velocity of the plugs, as well as the film thickness, and the distance between the plugs within a wide range of disperse and carrier phase flow rates. This allows constructing flow regime maps in microchannels using numerical simulations.

Author Contributions

Pryazhnikov M.I. planned the scheme, analyzed the experimental and numerical results; Minakov A.V. developed the mathematical modeling and carried out numerical simulation; Guzei D.V. conducted numerical modeling and analyzed results; Pryazhnikov A.I. conducted the experiments; Yakimov A.S. manufactured the chip. The manuscript was written through the contribution of all authors. All authors discussed the results, reviewed, and approved the final version of the manuscript.

Acknowledgment

We are grateful to the Krasnoyarsk Regional Shared Research Center (Krasnoyarsk Scientific Center, Siberian Branch, Russian Academy of Sciences) and Shared Research Center of Siberian Federal University for taking characterization of used fluids.

Conflict of Interest

The authors declared no potential conflicts of interest concerning the research, authorship, and publication of this article.

Funding

This paper is partially financed by the Ministry of Science and Higher Education of the Russian Federation (FSRZ-2020-0012).

Data Availability Statements

The datasets generated and/or analyzed during the current study are available from the corresponding author on reasonable request.

Nomenclature

Ca	Capillary number	Q	Volumetric flow rate [m^3/s]
D	Hydraulic diameter [m]	Re	Reynolds number
L	Length of plugs/droplets [m]	S	The cross-sectional area of micro-channel [m^2]
l_o	Distance between plugs/droplets [m]	St	Strouhal number
La	Laplace number	U	Characteristic velocity [m/s]
Oh	Ohnesorge number	We	Weber number



		Greek symbols	
μ	Viscosity [Pa s]	ρ	Density [kg/m ³]
Index			
c	continuous phase	o	oil
d	dispersed phase	w	water

References

- [1] Šalić, A., Tušek, A., Zelić, B., Application of microreactors in medicine and biomedicine, *Journal of Applied Biomedicine*, 10(3), 2012, 137–153.
- [2] Tran, T.M., Lan, F., Thompson, C.S., Abate, A.R., From tubes to drops: Droplet-based microfluidics for ultrahigh-throughput biology, *Journal of Physics D: Applied Physics*, 46(11), 2013, 114004.
- [3] Roberge, D.M., Ducry, L., Bieler, N., Cretton, P., Zimmermann, B., Microreactor Technology: A Revolution for the Fine Chemical and Pharmaceutical Industries?, *Chemical Engineering Technology*, 28(3), 2005, 318–323.
- [4] Sobhan, C.B., Garimella, S.V., A comparative analysis of studies on heat transfer and fluid flow in microchannels, *Microscale Thermophysical Engineering*, 5(4), 2001, 293–311.
- [5] Agostini, B., Fabbri, M., Park, J.E., Wojtan, L., Thome, J.R., Michel, B., State of the art of high heat flux cooling technologies, *Heat Transfer Engineering*, 28(4), 2007, 258–281.
- [6] Kandlikar, S.G., Fundamental issues related to flow boiling in minichannels and microchannels, *Experimental Thermal and Fluid Science*, 26(2-4), 2002, 389–407.
- [7] Kuznetsov, V.V., Shamirzaev, A.S., Kozulin, I.A., Kozlov, S.P., Correlation of the flow pattern and flow boiling heat transfer in microchannels, *Heat Transfer Engineering*, 34(2-3), 2013, 235–245.
- [8] Sattari-Najafabadi, M., Esfahany, M.N., Wu, Z., Sundén, B., Mass transfer between phases in microchannels: A review, *Chemical Engineering and Processing - Process Intensification*, 127, 2018, 213–237.
- [9] Mudawar, I., Two-phase microchannel heat sinks: Theory, applications, and limitations, *Journal of Electronic Packaging*, 133(4), 2011, 041002.
- [10] Foroughi, H., Kawaji, M., Viscous oil-water flows in a microchannel initially saturated with oil: Flow patterns and pressure drop characteristics, *International Journal of Multiphase Flow*, 37(9), 2011, 1147–1155.
- [11] Akbar, M.K., Plummer, D.A., Ghiasi, S.M., Gas-liquid two-phase flow regimes in microchannels, *ASME 2002 International Mechanical Engineering Congress and Exposition*, New Orleans, Louisiana, USA, IMECE2002-39555, 2002.
- [12] Dessimozi, A.L., Cavin, L., Renken, A., Kiwi-Minsker, L., Liquid-liquid two-phase flow patterns and mass transfer characteristics in rectangular glass microreactors, *Chemical Engineering Science*, 63(16), 2008, 4035–4044.
- [13] Kashid, M.N., Agar, D.W., Hydrodynamics of liquid-liquid plug flow capillary microreactor: Flow regimes, plug size and pressure drop, *Chemical Engineering Journal*, 131(1-3), 2007, 1–13.
- [14] Kashid, M.N., Renken, A., Kiwi-Minsker, L., Influence of flow regime on mass transfer in different types of microchannels, *Industrial & Engineering Chemistry Research*, 50(11), 2011, 6906–6914.
- [15] Zhao, Y., Chen, G., Yuan, Q., Liquid-liquid two-phase flow patterns in a rectangular microchannel, *AIChE Journal*, 52, 2006, 4052–4060.
- [16] Wu, Z., Cao, Z., Sundén, B., Liquid-liquid flow patterns and plug hydrodynamics in square microchannels of cross-shaped junctions, *Chemical Engineering Science*, 174, 2017, 56–66.
- [17] Kashid, M., Kiwi-Minsker, L., Quantitative prediction of flow patterns in liquid-liquid flow in micro-capillaries, *Chemical Engineering and Processing: Process Intensification*, 50(10), 2011, 972–978.
- [18] Waelchli, S., Rudolf von Rohr, P., Two-phase flow characteristics in gas-liquid microreactors, *International Journal of Multiphase Flow*, 32, 2006, 791–806.
- [19] Yagodnitsyna, A.A., Kovalev, A.V., Bilsky, A.V., Flow patterns of immiscible liquid-liquid flow in a rectangular microchannel with T-junction, *Chemical Engineering Journal*, 303, 2016, 547–554.
- [20] Yagodnitsyna, A.A., Kovalev, A.V., Bilsky, A.V., Experimental study of ionic liquid-water flow in T-shaped microchannels with different aspect ratios, *Journal of Physics: Conference Series*, 899(032026), 2017, 1–6.
- [21] Minakov, A.V., Shebeleva, A.A., Yagodnitsyna, A.A., Kovalev, A.V., Bilsky, A.V., Flow regimes of viscous immiscible liquids in T-type microchannels, *Chemical Engineering Technology*, 42, 2019, 1037–1044.
- [22] Darekar, M., Singh, K.K., Mukhopadhyay, S., Shenoy, K.T., Liquid-liquid two-phase flow patterns in Y-junction microchannels, *Industrial & Engineering Chemistry Research*, 56(42), 2017, 12215–12226.
- [23] Cox, R.G., The dynamics of the spreading of liquids on a solid surface. Part 1. Viscous flow, *Journal of Fluid Mechanics*, 168, 1986, 169–194.
- [24] Kistler SF. *Hydrodynamics of wetting*, Marcel Dekker, New York, 1993.
- [25] Shikmurzaev, Y.D., Moving contact lines in liquid/liquid/solid systems, *Journal of Fluid Mechanics*, 334, 1997, 211–249.
- [26] Lifton, V.A., Microfluidics: An enabling screening technology for enhanced oil recovery (EOR), *Lab on a Chip*, 16, 2016, 1777–1796.
- [27] Buchgraber, M., Clemens, T., Castanier, L.M., Kovscek, A.R., A microvisual study of the displacement of viscous oil by polymer solutions, *SPE Reservoir Evaluation and Engineering*, 14(03), 2011, 269–280.
- [28] Rangel-German, E.R., Kovscek, A.R., A micromodel investigation of two-phase matrix-fracture transfer mechanisms, *Water Resources Research*, 42(W03401), 2006, 1–13.
- [29] Sinton, D., Energy: The microfluidic frontier, *Lab on a Chip*, 14, 2014, 3127–3134.
- [30] Wang, L., Yang, S., Peng, X., Deng, H., Meng, Z., Qian, K., Wang, Z., Lei, H., An improved visual investigation on gas–water flow characteristics and trapped gas formation mechanism of fracture–cavity carbonate gas reservoir, *Journal of Natural Gas Science and Engineering*, 49, 2018, 213–226.
- [31] Yun, W., Ross, C.M., Roman, S., Kovscek, A.R., Creation of a dual-porosity and dual-depth micromodel for the study of multiphase flow in complex porous media, *Lab on a Chip*, 17, 2017, 1462–1474.
- [32] Minakov, A.V., Pryazhnikov, M.I., Suleymanna, Y.N., Meshkova, V.D., An experimental study of the effect of the addition of silicon oxide nanoparticles on the wettability characteristics of rocks with respect to oil, *Technical Physics Letter*, 46(12), 2020, 1238–1240.
- [33] Minakov, A.V., Pryazhnikov, M.I., Suleymanna, Y.N., Meshkova, V.D., Guzei, D.V., Experimental study of nanoparticle size and material effect on the oil wettability characteristics of various rock types, *Journal of Molecular Liquids*, 327, 2021, 114906.
- [34] Minakov, A.V., Rudyak, V.Y., Pryazhnikov, M.I., Systematic experimental study of the viscosity of nanofluids, *Heat Transfer Engineering*, 42(12), 2021, 1024–1040.
- [35] Behroodi, E., Latifi, H., Bagheri, Z., Ermis, E., Roshani, S., Moghaddam, M.S., A combined 3D printing/CNC micro-milling method to fabricate a large-scale microfluidic device with the small size 3D architectures: an application for tumor spheroid production, *Scientific Reports*, 10(22171), 2020, 1–14.
- [36] Matellan, C., del Río Hernández A.E., Cost-effective rapid prototyping and assembly of poly(methyl methacrylate) microfluidic devices, *Scientific Reports*, 8(6971), 2018, 1–13.
- [37] Hirt, C.W., Nichols, B.D., Volume of fluid (VOF) method for the dynamics of free boundaries, *Journal of Computational Physics*, 39(1), 1981, 201–225.
- [38] Brackbill, J.U., Kothe, D.B., Zemach, C., A continuum method for modeling surface tension, *Journal of Computational Physics*, 100(2), 1992, 335–354.
- [39] Minakov, A.V., Numerical algorithm for moving-boundary fluid dynamics problems and its testing, *Computational Mathematics and Mathematical Physics*, 54(10), 2014, 1560–1570.
- [40] Garstecki, P., Fuerstman, M.J., Stone, H.A., Whitesides, G.M., Formation of droplets and bubbles in a microfluidic T-junction - Scaling and mechanism of break-up, *Lab on a Chip*, 6, 2006, 437–446.
- [41] Xu, J.H., Li, S.W., Tan, J., Luo, G.S., Correlations of droplet formation in T-junction microfluidic devices: From squeezing to dripping, *Microfluidics and Nanofluidics*, 5, 2008, 711–717.
- [42] Li, Q., Angelis, P., Experimental and numerical hydrodynamic studies of ionic liquid-aqueous plug flow in small channels, *Chemical Engineering Journal*, 328, 2017, 717–736.
- [43] Cao, Z., Qian, J.Y., Wu, Z., Sundén, B., Water-oil flow in square microchannels with a crossed junction, *ASME 2018 5th Joint US-European Fluids*



Engineering Division Summer Meeting, Montreal, Quebec, Canada, FEDSM2018-83056, 2018.

[44] Sobieszuk, P., Cygański, P., Pohorecki, R., Bubble lengths in the gas-liquid Taylor flow in microchannels, *Chemical Engineering Research and Design*, 88, 2010, 263–269.

[45] Fu, T., Ma, Y., Funfschilling, D., Zhu, C., Li, H.Z., Squeezing-to-dripping transition for bubble formation in a microfluidic T-junction, *Chemical Engineering Science*, 65(12), 2010, 3739–3748.

[46] Minakov, A.V., Rudyak, V.Y., Gavrilov, A.A., Dektere, A.A., Mixing in a T-shaped micromixer at moderate Reynolds numbers, *Thermophysics and Aeromechanics*, 19(3), 2012, 385–395.

[47] Lobasov, A.S., Minakov, A.V., Analyzing mixing quality in a T-shaped micromixer for different fluids properties through numerical simulation, *Chemical Engineering and Processing: Process Intensification*, 124, 2018, 11–23.

ORCID iD

M.I. Pryazhnikov  <https://orcid.org/0000-0001-9143-7950>

A.V. Minakov  <https://orcid.org/0000-0003-1956-5506>

D.V. Guzei  <https://orcid.org/0000-0003-2226-1837>

A.I. Pryazhnikov  <https://orcid.org/0000-0002-6124-037X>

A.S. Yakimov  <https://orcid.org/0000-0003-4919-9877>



© 2022 Shahid Chamran University of Ahvaz, Ahvaz, Iran. This article is an open access article distributed under the terms and conditions of the Creative Commons Attribution-NonCommercial 4.0 International (CC BY-NC 4.0) license (<http://creativecommons.org/licenses/by-nc/4.0/>).

How to cite this article: Pryazhnikov M.I., Minakov A.V., Guzei D.V., Pryazhnikov A.I., Yakimov A.S. Flow Regimes Characteristics of Water-crude Oil in a Rectangular Y-microchannel, *J. Appl. Comput. Mech.*, 8(2), 2022, 655–670.
<https://doi.org/10.22055/JACM.2021.38784.3282>

Publisher's Note Shahid Chamran University of Ahvaz remains neutral with regard to jurisdictional claims in published maps and institutional affiliations.

